Proceedings of the
International Conference on Mechanical Engineering 2009
(ICME2009) 26- 28 December 2009, Dhaka, Bangladesh

ICME09-FM-04

EXPERIMENTAL STUDY OF FRACTAL TURBULENCE

S.M. Muztaba Salim, **F.C.G. Nicolleau** , **M. Borkowski**

University of Sheffield, Dept of mechanical Engineering, UK

ABSTRACT

Fractal turbulence is deemed much more efficient than grid turbulence in terms of the flow mixing properties. In this paper, we present our hotwire experimental results of fractal turbulence generated by fractal orifice. The self-similar edge characteristic of the fractal orifice is thought to play the vital role in the enhanced mixing properties. We used four fractal orifices, each paired with a smooth orifice of equivalent flow area. The objectives were two folds, the first was to study the fractal scaling influence on the flow and the second was to explore the potential of the fractal orifice flow meter to determine the flow rate in a pipe. The results provided an excellent insight of the fractal generated turbulence and the fractal flow physics. Across the fractal orifice, the pressure drop was lower but the turbulence intensity was higher than those across the paired smooth orifice.

Keywords: Fractal, Turbulence, Hotwire.

1. INTRODUCTION

Study of fractal property can be traced back to as far as 650 AD in the page design layout of the *Book of Durrow*, Ireland. Yet the term *fractal* was first coined by the famous Polish Mathematician, Benoît Mandelbrot, only in 1975. His difficulty in describing the shapes in details at various scales made him pick the word, *fractal,* where the Euclidean geometries such as triangle, rectangle or a circle did not fit to do the job. Take a tree for example. In a three dimensional world, the shape of a tree can be roughly visualized as a sphere on top of a cylinder or in a two dimensional world, the same tree can be viewed as a circle on the top of a long narrow rectangle. But how about when we try to describe the same tree in its micro scale, i.e., how its branches bifurcate or how is the distribution of the leaves? Here comes the fractal property as a savior. Another famous example is the cauliflower. Any smaller portion of it resembles the exact whole of it no matter how many times the same dissection is repeated.

Fractal geometry, as defined in [1], is a derivative of classical Euclidean geometry characterized by infinite detail where the edge smoothness is absent. Mandelbrot [2] defined the fractal property to be the self similar infinite repetition of the whole object from macro to micro scale.

The above definitions can easily be realized in the case of any turbulent flow. In a turbulent flow, the flow pulsations of lower order, mentioned by Kolmogrov [3], absorb energy of the motion and transfer it to the higher order pulsations until the finest pulsation is overcome by the flow viscosity. Stewart [4] mentioned this as energy cascade and showed that only under certain circumstance the flow becomes turbulent. The turbulent flow takes energy from the large scales which themselves are unstable and break into smaller scales. However, during the breaking process the self similarity of the structures are preserved. This evidently represents the fractal characteristic of the turbulence.

Despite the inherent fractal property of turbulence, very few attempts have been made to generate turbulence by fractal grids as opposed to usual grid turbulence [5, 6, 7] where the grids are evenly distributed. The turbulence generated by fractal grids is referred to as fractal turbulence. Kearney [8] tried to exploit the fractal property of the turbulence in fluid scaling. He engineered a 3D fractal grid to create low energy fractal turbulence to control the geometry of fluid scaling process and implemented it in molasses chromatography process successfully. Queiros-Conde and Vassilicos [9] found that by using the fractal grids a well developed turbulence can be generated. When the fractal dimension is increased the velocity fluctuations tend to be more evenly distributed. More about the fractal dimension may be found in [10]. Staicu *et al.* [11] demonstrated that the flow is significantly affected by the orientation of the fractal grid. To illustrate the influence of the fractal grid on the flow, they compared their results with non-fractal grid turbulence. Keylock *et al*. [12] studied fractal fences, a variant of fractal grids and postulated that the use of fractal fences may suppress the high wind to protect flash flood or avalanche. Seoud and Vassilicos [13] concluded that using the fractal grids as higher as three times turbulence intensities may be produced than classical non fractal grids. They also concluded that their space filling fractal square grids generated a kind of

homogeneous isotropic turbulence whose decays locked into a single length scale. Hurst and Vassilicos [14] conducted an extensive work on 21 planar fractal grids to study scaling and decay of fractal turbulence. They found that the turbulence decay is strongly dependent on the fractal dimension, effective grid mesh size and the ratio between the largest to smallest bar thickness. However, the use of the fractal turbulence was never attempted in the pipe flow until very recently some attempts were made to associate the fractal turbulence with the orifice flow meter [15,16]. A flow meter is a device which is used to determine the flow rate in a pipe flow. With an orifice flow meter, the pressure drop across the orifice is measured. Then the flow rate can be calculated by the flow area of the orifice. The motivation behind this present work arose from the two practical points. One from the engineering point of view is to explore the potential of fractal orifice meter to determine the flow rate in a pipe and the other is from the point of understanding the fractal scaling effect.

2. EXPERIMENTAL SET UP

The following sections describe the experimental set up covering the details of the measurement.

2.1 Fractal vs. Smooth Orifices

As mentioned in the preceding section, a fractal orifice is a flow meter at its simplest form. The popular Koch curve by the famous Swedish mathematician Helge Von Koch (1870-1924) was adopted to design the fractal orifice shown in Fig. 1.

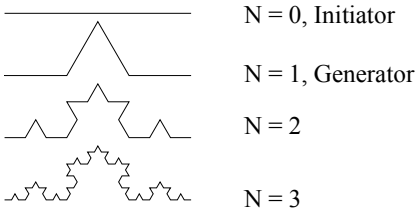

Fig 1. The Koch Curve was constructed by the Swedish Mathematician Von Koch in 1904

The inner edge of the orifice used in this experiment had the characteristics of the Koch curve. At each iteration, the edge lost the "smoothness" and the flow area increased. On the other hand, a smooth orifice is the one whose inner edge is smooth, a very distinguishable characteristic than that of the fractal orifice. Like the fractal orifice, the flow area of the smooth orifice is also increased at each iteration. The total area after each iteration was calculated by the following formula:

$$A_N = A_0\left[1+\frac{1}{3}\sum_{i=0}^{N-1}\left(\frac{4}{9}\right)^i\right] \qquad (1)$$

Where A_N = total area after one iteration, A_0 = area after previous iteration, N = number of iteration step. Fig. 2 shows the fractal orifices, each combined with a smooth orifice of equivalent flow area. The outer diameter of the orifice was 140.8 mm which was kept constant for each orifice. The orifice was made of aluminum and had a thickness of 2 mm. For the naming purpose, we adopted the following convention that would be used throughout this paper; F0 was the fractal orifice at the zero-*th* iteration, while F1 was the fractal orifice after first iteration and so on. Similarly, S0 was the smooth orifice at the zero-*th* iteration and S1 was the smooth orifice after first iteration and so on. The pairs were F0-S0, F1-S1, F2-S2 and F3-S3, as shown in Fig. 2. Each pair had an equivalent flow area.

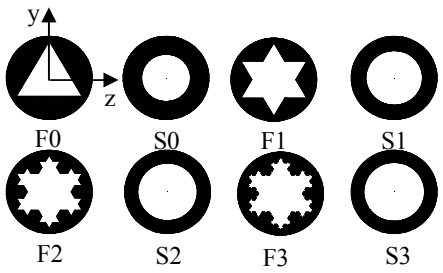

Fig 2. Four fractal orifices, N = 0 - 3, each paired with a smooth orifice of equivalent flow area

It is to bear in mind that the fractal orifice (N = 0) at the zero-*th* iteration was not essentially a fractal orifice but involved only one scale and hence it was topologically the same as a circular smooth orifice except that some roughness was introduced through the triangle apex.

2.2 Wind Tunnel

The wind tunnel used in the experiment had a bell-mouth inlet for uniform flow and reduced inlet pressure losses [16]. The schematic of the wind tunnel is shown in Fig. 3. It had a working section of 3820 mm length and the inner diameter of 140.8 mm and was made of 5 mm thick polycarbonate. A motor driven fan was used to "suck down" the ambient air into the tunnel through the bell mouth and leave through a controlling valve. The controlling valve could be regulated to achieve the desired flow velocity in the tunnel. A maximum of 17 m/s flow velocity could be attained by the electric motor fitted at the other end of the tunnel. The motor had a rating of 372.85 J with a speed of 2850 rpm.

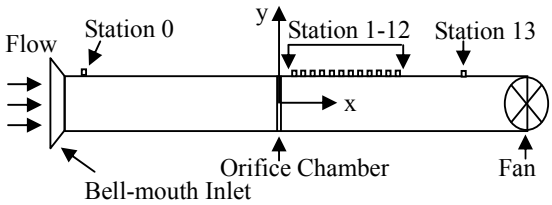

Fig 3. Bell-mouth wind tunnel

The orifice chamber was located 14.50*D* away from the entrance. Of the fourteen Stations, one was 14.15*D* upstream of the orifice chamber near the entrance, named Station 0, and one was 13*D* downstream of the orifice chamber, named Station 13. The remaining twelve

Stations were immediately behind the settling chamber. The first Station of the twelve was 1*D* behind the orifice chamber, named Station 1, followed by Station 2 to Station 12. The distance between the two successive remaining Stations was 0.04*D* from Station 1 to 12. Each Station was further divided into 15 Substations (A to N) vertically from the wall to the center of the tunnel each with 5 mm apart. The Substation xA was located at the wall and the Substation xN was located at the center of the tunnel where x was any Station.

2.3 Experimental Devices

A constant temperature type hotwire system manufactured by Dantec Dynamics (Model 54T30 miniCTA) together with the hotwire probe (Model 55P16) from the same manufacturer was used to collect the velocity data. The output signal from the anemometer was continuously analogue. An analog-to-digital converter from the National Instrument (Model PCI-6023E) was used to obtain the digital signal. This anemometer allowed only one input from the hotwire and one output to a digital analogue converter. It was equipped with a Wheatstone bridge circuit connected to a servo-amplifier, signal conditioner, low-pass filter and dipswitches. It was necessary to do this when the hotwire probe was changed and the new one had different resistance or when the ambient fluid temperature had changed a lot. Overheat ratio was the ratio between the wire resistivity when warmed up and the resistivity at room temperature, 20 °C. This overheat ratio was defined by the temperature at which the wire ws maintained during operation. During measurements overheat ratio was 1.8. Dipswitches were adjusted according to the spreadsheet supplied by Dantec. TSI 1125 calibrator and Furness FC0510 micro manometer was used during the calibration. The manometer was capable of measuring 2000 to 0.001 Pa.

2.4 Experimental Procedures

Prior to the data collection during each measurement, hotwire calibration was done to ensure reliable data.

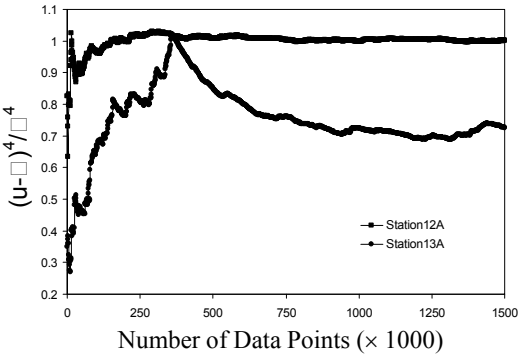

Fig 4. Convergence test to decide the sufficient number of data points for the velocity measurement

Each measurement was carried out at a maximum frequency of 10 kHz. To decide the number of hotwire sampling data for each point, a velocity convergence test was conducted at Station 12 and Station 13. We randomly picked fractal orifice F2 for the convergence test. A total of 3×10^6 velocity data was measured. The convergence test was done in the following way. We averaged the first 100,000 data points, then the first 200,000 data points, then the first 300,000 and so on until all 3×10^6 data were covered. Finally we constructed the "number of data vs velocity curve". Fig. 4 shows the fourth order velocity fluctuation normalized by the mean velocity as a function of the number of data point plot from the convergence test and we decided that 1×10^6 data would be sufficient to get the velocity information without jeopardizing the accuracy. The velocity measurement was limited to the one half of the tunnel diameter assuming the flow had a radial symmetric profile as it was a circular wind tunnel. The flow rate at each measurement run was kept constant by regulating the control valve adjusting the mass flow rate. The inlet velocity was 9.75 m/s. Figure 5 shows the pdf of the inlet velocity. The Reynolds number was 95,000 based on the tunnel diameter.

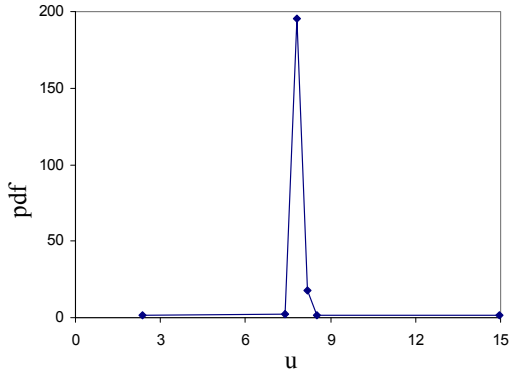

Fig 5. PDF of inlet velocity at Station 0

The pressure measurements were conducted at constant flow rate. The pipe connections between the Stations and the pressure measuring device were carefully checked to avoid any pressure leakage. Prior to each measurement, the flow was initiated and let it run for an appreciated time to ensure the tunnel was filled with the working fluid in motion. The pressure drops were measured between the Station 0 and the Station 13 across both the fractal and smooth orifices.

2.5 Normalization

In order to normalize both the pressure drop and velocity, we used the following two equations,

$$\Delta p_{norm} = \frac{2\Delta p}{\rho U_{inlet}^{\ 2}\left(\frac{A}{A_i}\right)} \tag{2}$$

and

$$U_{norm} = \frac{\overline{U}}{U_{inlet}\left(\frac{A}{A_i}\right)} \tag{3}$$

where, Δp_{norm} was the normalized pressure, Δp was

the pressure drop in Pa, ρ was the density of the working fluid which was air in our case, A was the area of the wind tunnel cross section, A_i was the flow area of the orifice, the index-i represents the number of iteration, U_{norm} was the normalized velocity and U-*bar* was the average velocity.

3. ERROR ANALYSIS

Two types of measurements were conducted. One was the hotwire measurement and the other one was the pressure measurement. Below a brief description of the related errors are given.

3.1 Hotwire Measurement Error

Errors associated with hotwire measurement could be further divided into two categories.

3.1.1 Global Error

These inherent errors were always present regardless of any special care taken mostly due to the commonly known limitations associated with hotwire measurement technique such as the intrusive nature of the technique itself. The flow was always disrupted by the probe. We assumed that because of the high Reynolds number (Re_D = 9.55 x 10^4) this error was negligible.

Another error was the gradual decrease of the probe performance which was a function of time. We had fourteen Stations each with fifteen Substations. For eight orifices and the number of data points of 1000,000 made, it was impossible to run the experiments in one go to comply with the ideal measurement practice. To tackle this, we divided the experiments in several days. It is to be noted that hotwire measurements are highly sensitive to ambient temperature, humidity and air pressure. Keeping them in mind we took extra care and in some cases used two different probes.

3.1.1 Local Error

These errors were due to the limitation of the experimental set up. The probe properties were also very sensitive to micro size dust when used for a longer period. To handle the dust problem, we tried to install air filter at the bell-mouth inlet. But this dramatically increased the pressure drop across the filter due to its low filter face velocity. The motor induced vibration also affected the velocity measurement. Although the vibration had negligible influence on the measurement but at the time of measurement, complete removal or isolating the vibration failed due to the set up limitation.

3.2 Pressure Measurement Error

The pressure drop, Δp, calculated always had a fluctuation of about ± 20 *Pa* due to the negligible vibration induced by the motor fan. To minimize the error, an average was taken over the several measurements.

$$\sigma_r = \frac{\left\langle \left(\Delta p - \langle \Delta p \rangle\right)^2 \right\rangle^{\frac{1}{2}}}{\langle \Delta p \rangle} \qquad (4)$$

Applying Equation 4 the relative pressure r.m.s. σ_r was used to determine the relative error for each measurement. The maximum r.m.s. value did not exceed 4.3%. To further minimize the pressure error, the differential pressure, p, was averaged over twenty seconds. This significantly improved the pressure measurements.

4. RESULTS AND DISCUSSIONS

The objectives of this experimental work were two folds, the first: to understand the fractal scaling effects on the flow and the second: to distinguish the fractal orifice induced flow properties from the smooth orifice. We conducted both velocity and pressure measurements separately. In the following section, some key findings will be reported and discussed.

4.1 Pressure Measurements

Two sets of pressure measurements were done. The first set was to measure the pressure drops across the fractal and smooth orifices between Station 0 and Station 13 and the second set was to measure the atmospheric pressure drops for all the twelve stations, from Station 1 to Station 12. Both fractal and smooth orifices, N = 0 – 3, were used and this allowed a direct comparison between them and thus the study of the fractal scaling properties were possible. Fig. 6 shows the pressure drops across the fractal and the smooth orifices between Station 0 and Station 13. The pressure drop was higher for both the fractal and the smooth orifices at the zero-*th* iteration but significantly increased after first iteration. As the number of the fractal iteration increased the pressure drop recovery was observed or at least remained constant.

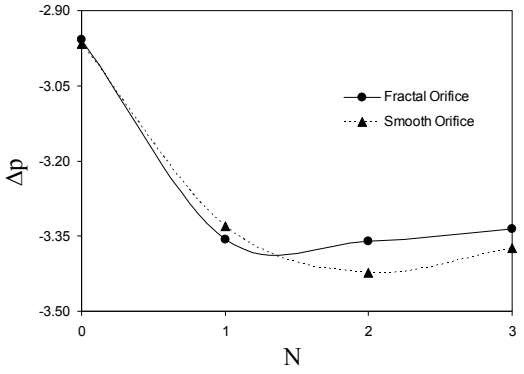

Fig 6. Pressure drops across the fractal and smooth orifices. The x-axis shows the number of iteration.

It could be intuitively said that with the increase of the number of the iterations, the pressure drop curve would show an asymptotic behavior. Also it was observed from Fig. 6 that the pressure drop was lower for the fractal orifice than for the smooth orifice. This was much more pronounced at the second iteration and was an indication that across the fractal orifice flow recovery occurred faster than across the smooth orifice. This could be further verified from Fig. 7, where x-axis was the position behind the orifice from Station 1 to Station 12. The fractal orifices induced lower pressure drops than their counterparts and as seen in Fig. 6, pressure drop dramatically reduced after the first iteration. The further

the downstream position was, the faster the flow recovered as expected. For the fractal orifices, this recovery was quicker than the smooth orifices. Also, the lower pressure drop behind the fractal

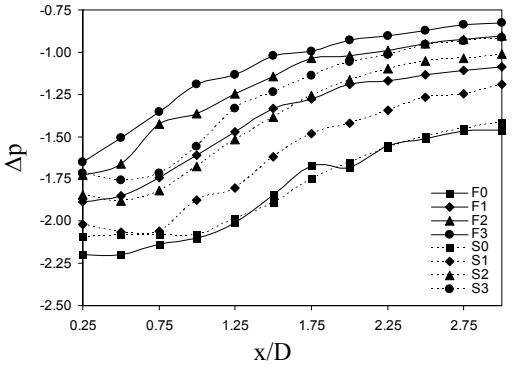

Fig 7. Normalized pressure drops behind the fractal and the smooth orifices at different stations

orifice was consistent at each iteration and downstream Station to a good extent. This was an obvious indication that the fractal scaling had significant effects on the flow properties which enhanced the mixing leading to a pressure reduction and a faster flow recovery. The results also showed that the differences in pressure drops between the fractal and the smooth orifices reduced as the iteration number reached to the higher one. From this it was deduced that as the number of iteration would increase the characteristics of the fractal orifices would asymptote the characteristics of the smooth orifice and the flow would continue independent of the orifice types.

4.2 Hotwire Measurements

We measured velocity at each Station and its Substations.

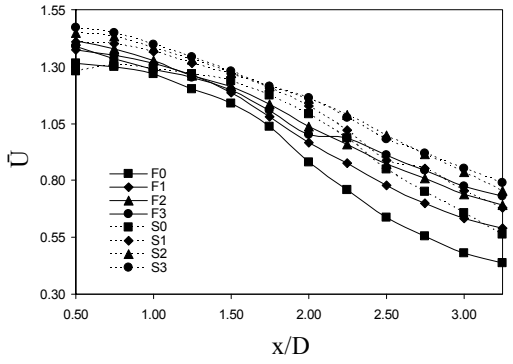

Fig 8. Mean velocity at centerline

Fig. 8 shows the mean velocity distribution along the centerline of the tunnel from Station 1 to Station 12. The solid lines correspond to the fractal orifices and the dashed lines correspond to the smooth orifices. It was clearly noticeable that the fractal orifices created smaller velocity scales than that of the smooth orifice. On the other hand from Fig. 9, we see that the fractal orifices created larger range of the scales of the flow structures.

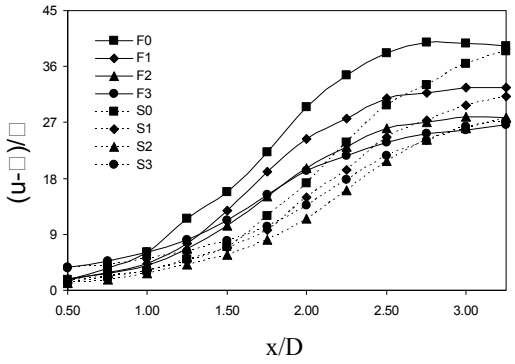

Fig 9. Turbulence Intensity at centerline

This was the process that initiated energy cascades leading to a better flow mixing properties. This also explained the lower pressure drop across the fractal orifices in contrast with the smooth orifice. Fig. 10 shows the velocity pdf at Station 12 downstream the orifice chamber. From the top left corner, clockwise, the pdfs clearly confirm that the larger range of velocity scales for fractal orifices were associated with the fractal scaling in comparison with the smooth orifices.

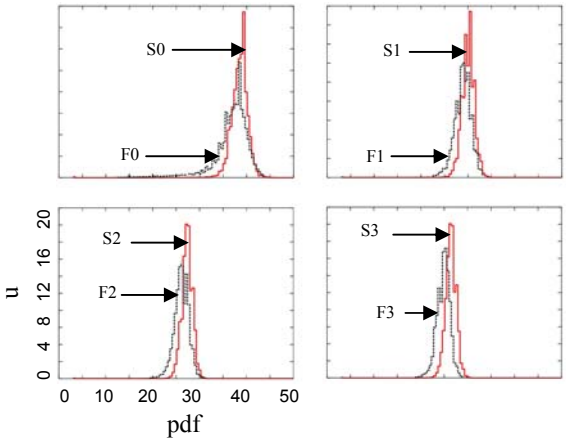

Fig 10. Velocity pdf at Station 12 across both the fractal and smooth orifices

5. CONCLUSION

An experimental study of the fractal turbulence was conducted in an open circular wind tunnel. Hotwire measurement technique was implemented for the study. Both the fractal and the smooth orifices of equivalent flow area were used. The following conclusions were drawn from the results. Across the fractal orifice, as opposed to the smooth orifice,

1. flow mixing enhanced,
2. pressure drop lowered,
3. velocity scale decreased and
4. range of different velocity scales increased.

These were the clear indication of the influence of the fractal characteristics of the fractal orifice.

At the zero-th iteration, similar flow properties were

observed across both the fractal and smooth orifice. This was because at the zero-th iteration, the edge of the fractal orifice was not actually fractal. Topologically, it was just another smooth orifice except some friction was introduced by the sharp triangle apex as opposed to the smooth circular orifice of the equivalent flow area. As the number of iteration of fractal scaling increased, the flow properties were influenced by the fractal edge which was clearly distinguishable from the smooth orifice. It was assumed that at further higher iteration, the flow properties again would become identical to that of the smooth orifice.

6. REFERENCES

1. Nigel Lesmoire-Gordon, Will Rood and Ralph Edney, 2000, "Introducing Fractal Geometry", Icon Books, UK
2. Mandelbrot, J., 1974, "On the Geometry of Homogeneous Turbulence with Stress on the Fractal Dimension of the Iso-Surfaces of a Scalar, Journal of Fluid Mech., 72 (2), 401-416
3. Kolomogorov, A. N., 1941, "The Local Structure of Turbulence in Incompressible Viscous Fluid for Very Large Reynolds Numbers", C. R. Acad. Sci. U.R.S.S. 30, 301
4. Stewert, R.W., 1969, "Notes on Turbulence", NASA No. 21626
5. Salim, S.M.M., Saga, T. and Taniguchi, N., 2004, "Experimental Analysis of the Control of Turbulent Intensity in a Square Channel", The Japan Society of Mechanical Engineers 10, pp. 563-564
6. Zwart, P.J., Budwig and Tavoularis, S., 1997, "Grid Turbulence in Compressible Flow", Experiments in Fluids 23, 520-522
7. Antonia, R.A. and Burattini, P., 2006, Approach to the 4/5 Law in Homogeneous Isotropic Turbulence, J. Fluid Mech. 550, pp. 175-184.
8. Kearney, M., Kochergin, V. Petersen, K., Mumm, M., Jacob, W. and Velasquez, L., 1999, "Applications of Engineered Fractals in the Sugar Industry", Amalgamated Research Inc. ASSBT.
9. Queiros-Conde, D. and Vassilicos, J. C., 2000, "Intermittency in Turbulence and Other Dynamical Systems", Chapter: Turbulent wakes of 3-D fractal grids, Cambridge University Press.
10. http://math.bu.edu/DYSYS/chaos-game/node6.html
11. Staicu, A. et al., 2003, "Turbulent wakes of fractal objectes", Physical Review E 67, 066306.
12. Keylock C. and McElwaine J. 2005, "Understanding snow avalanches: Recent progress from a British perspective", Presented at the 2005SET for BRITAIN meeting for younger British scientists and engineers, House of Commons.
13. Seoud, R. and Vassilicos, J., 2007, Dissipation and Decay of Fractal-generated Turbulence, Physics of Fluids 19, 105108
14. Hurst, D. and Vassilicos, J., 2007, "Scaling and Decay of Fractal-generated Turbulence", Physics of Fluids, 19, 035103
15. Ahmadi, A. 2006, "The swirling orifice plate independent of inlet conditions", PhD Thesis, University of Sheffield, Department of Mechanical Engineering.
16. Abou-El-Azm, A. et al., 2009, "Experimental study of the pressure drop after fractal orifices in turbulence pipe flows", Exp. in Fluid & Thermal Science, (In Press).
17. Mehta, R.D. and Bradshaw, P., 1979, "Design Rules for Small Low Speed Wind Tunnels", The Aero. J. of the Royal Aero. Soc., Technical Notes.

5. MAILING ADDRESS

S.M. Muztaba Salim
University of Sheffield,
Dept of mechanical Engineering,
Mapping Street, Sheffield S13JD, UK